HHS Public Access

Author manuscript

Mol Nutr Food Res. Author manuscript; available in PMC 2018 May 01.

Published in final edited form as:

Mol Nutr Food Res. 2017 May ; 61(5): . doi:10.1002/mnfr.201600576.

Lack of β, β-carotene -9', 10'-oxygenase 2 leads to hepatic mitochondrial dysfunction and cellular oxidative stress in mice

Lei Wu[1], **Xin Guo**[1], **Steven D. Hartson**[2], **Mary Abby Davis**[1], **Hui He**[1], **Denis M. Medeiros**[3], **Weiqun Wang**[4], **Stephen L. Clarke**[1], **Edralin Lucas**[1], **Brenda J. Smith**[1], **Johannes von Lintig**[5], and **Dingbo Lin**[1]

[1]Department of Nutritional Sciences, Oklahoma State University, Stillwater, OK

[2]Department of Biochemistry and Molecular Biology, Oklahoma State University, Stillwater, OK

[3]Graduate School, University of Missouri-Kansas City, Kansas City, MO

[4]Department of Food, Nutrition, Dietetics, and Health, Kansas State University, Manhattan, KS

[5]Department of Pharmacology, Case Western Reserve University, Cleveland, OH

Abstract

Scope—β,β-carotene-9',10'-dioxygenase 2 (BCO2) is a carotenoid cleavage enzyme localized to the inner mitochondrial membrane in mammals. This study was aimed to assess the impact of genetic ablation of BCO2 on hepatic oxidative stress through mitochondrial function in mice.

Methods and Results—Liver samples from 6 week old male $BCO2^{-/-}$ knockout (KO) and isogenic wild-type (WT) mice were subjected to proteomics and functional activity assays. Compared to the WT, KO mice consumed more food (by 18 %) yet displayed significantly lower body weight (by 12 %). Mitochondrial proteomic results demonstrated that loss of BCO2 was associated with quantitative changes of the mitochondrial proteome mainly shown by suppressed expression of enzymes and/or proteins involved in fatty acid β–oxidation, the tricarboxylic acid cycle, and the electron transport chain (ETC). The mitochondrial basal respiratory rate, proton leak, and ETC complex II capacity were significantly elevated in the livers of KO compared to WT mice. Moreover, elevated reactive oxygen species and increased mitochondrial protein carbonylation were also demonstrated in liver of KO mice.

Conclusions—Loss of BCO2 induces mitochondrial hyperactivation, mitochondrial stress and changes of the mitochondrial proteome, leading to mitochondrial energy insufficiency. BCO2 appears to be critical for proper hepatic mitochondrial function.

Corresponding author: Dingbo Lin, PhD, Department of Nutritional Sciences, Oklahoma State University, Stillwater, OK 74078, USA, Phone:1-405-744-5215, Fax: 1-405-744-1357, dingbo.lin@okstate.edu.

Author contributions

DMM, WW, SLC, EL, BJS, JL, and DL designed the study; LW, XG, SH, KP, AD, and HH conducted the research; LW, SH, KP analyzed the data; LW, DMM, WW, SLC, EL, BJS, JL, and DL wrote and revised the manuscript; and LW and DL had primary responsibility for final content. All authors read and approved the final manuscript.

Conflict of interest

All authors have no conflicts of interest

Keywords

β, β-carotene -9', 10'-oxygenase 2 (BCO2); electron transport chain; liver; mitochondrial dysfunction; mitochondrial proteome; oxidative stress

Introduction

The imbalance between the systemic production of reactive oxygen species (ROS) and the systemic capacity to quench and/or detoxify ROS production results in oxidative stress (1, 2). ROS can damage many cellular components, such as lipids, proteins, and nucleotides (3). Mitochondria are the power "engine" of the cell involved in numerous cellular processes including redox homeostasis, cellular signaling, development, growth, differentiation and even cell death (4–6). Leakage of protons and/or electrons from the mitochondrial electron transport chain (ETC) results in enhanced generation of ROS and subsequent mitochondrial oxidative stress and decreased efficiency of ATP production, cellular oxidative stress (7) and subsequent inflammation (8). Mitochondrial oxidative stress has been well established as a causal factor in the development of chronic diseases, such as diabetes (9–11) and obesity (12). In diabetes, oxidative stress is associated with tissue-specific changes of the mitochondrial proteomes (13), impaired insulin function and disrupted blood glucose control (14, 15). Additionally, systemic oxidative stress is closely associated with chronic diseases, such as obesity in humans (16). Thus, properly functioning of mitochondria is crucial for the maintenance of cellular homeostasis in mammals.

β, β-carotene-9', 10'-oxygenase 2 (BCO2), a carotenoid cleavage enzyme that is conserved in primates, catalyzes the asymmetrical cleavage of carotenoids at 9', 10' and 9, 10 double bond to form various apocarotenoid cleavage products (17,18,19). Interestingly, in humans the *BCO2* gene locus is closely linked to the proinflammatory mediator interleukin-18 (IL-18) (20). Variants at the *BCO2* locus are associated with the IL-18 level, but not carotenoids in either plasma or macula (20). Studies have revealed that mutations in human *BCO2* have been linked to macular degeneration (21), insulin resistance and obesity (22), and prostate cancer (23). Further, the loss of BCO2 protein expression is associated with the development of anemia in zebrafish, though the anemia results not from impaired erythropoiesis, but instead from increased apoptosis of erythrocyte precursors (24). BCO2 expression is also significantly reduced in obese and diabetic mice (25, 26) . Accordingly, increased intake of a high-fat diet rich in carotenoids increase the expression of BCO2 protein and was associated with increased insulin sensitivity and attenuation of fatty liver in obese C57BL/6J mice (25). Collectively, these findings indicate that BCO2 likely plays roles other than just as a carotenoid cleavage enzyme in mammals.

BCO2 is widely expressed in many types of tissues and is localized to in the inner mitochondrial membrane (18, 27, 28). Exogenous H_2O_2 induces BCO2 protein expression in HepG2 cells though the function of this protein under oxidative stress is not clear (29). Lutein and/or zeaxanthin-enriched diets cause hepatic mitochondrial dysfunction in BCO2 KO mice due to oxidative stress induced by accumulation of carotenoids (29). The role of BCO2 in retinal carotenoid metabolism is still controversial (17, 19). It remains unknown

whether BCO2 functions as a structural protein in the mitochondrial homeostasis. In this study, the liver tissues of wild type (WT) and $BCO2^{-/-}$ knockout (KO) mice fed a standard chow diet were analyzed by mitochondrial proteome profiling and functional activity assays, production of reactive oxygen species (ROS), and mitochondrial protein carbonylation. We sought to determine whether BCO2 protein was critical to mitochondrial function in liver, and to investigate how ablation of BCO2 caused hepatic mitochondrial dysfunction and triggers cellular oxidative stress.

Materials and methods

Animals, animal care and fasting blood glucose test

The original BCO2 knockout mouse (29) was backcrossed to the wild-type 129S6 (WT) for seven generations to obtain a $BCO2^{-/-}$ knockout (KO) strain in a 129S6 genetic background (Taconic, New York). The breeding colonies of both WT and KO strains were maintained in the Animal Resources Facility at Oklahoma State University. After weaning at 21 days, mice had free access to water and food (e.g., *ad libitum*) throughout the study. All animal experiments and procedures were performed in accordance with our protocol approved by the Oklahoma State University Institutional Animal Care and Use Committee (OSU IACUC protocol # HS-14-4). Male mice were group-housed (3 mice/cage) in a controlled environment with a 12-h light/dark cycle (7:00 -19:00 light/19:00-7:00 dark) and fed a standard chow diet for 3 weeks (CD, 10% kcal from fat, catalog # D12450B, Research Diets, Inc., New Brunswick, NJ). The macronutrient composition of the CD is 10% kcal from fat, 20% kcal from protein, and 70% kcal from carbohydrate. Food intake and body weight were monitored weekly at 8:30-9:30 AM starting at weaning (at 3 weeks of age) to 6 weeks of age (n=12). The mean of weekly food intake between 5 and 6 weeks and the body weight at 6 weeks of age were presented. WT and KO mice at 6 weeks of age were used for tissue collection and laboratory analysis. Animals were sacrificed by CO2 at 8:30-9:30 AM for experiments after being fasted for 5-6 hr. Before necropsy, the fasting blood glucose was tested by tail snip using the Precision Xtra blood glucose monitoring system (Alameda, CA, USA).

Measurement of plasma free fatty acids (FFA)

Plasma FFA was analyzed using a BioLis 24i automated analyzer (Carolina Chemistry, NC, USA). The FFA level is expressed as milliequivalents per liter (mEq/L).

Cellular ROS level

The hepatic ROS level was measured using dichlorodihydrofluorescein (DCF) as previously described (26). Briefly, 25 μL carboxy-DCF and H_2-DCF dyes at 125 μmol/L were added into freshly prepared liver homogenates (100 μg protein/100 μL probes) in a 96-well plate. Changes in fluorescence intensity were recorded by the Bio-Tek Synergy HT fluorescence microplate reader (Winooski, VT) at excitation 485 nm/emission 530 nm. The ROS level was expressed as increased absorbance values (relative fluorescent unit OD 485/530, OD at 45 min - OD at 0 min).

Hepatic mitochondrial isolation

After euthanization, liver tissue were immediately used to assess mitochondrial function. Approximately 60 mg liver tissue was minced in 0.5 mL mitochondrial isolation buffer at pH 7.2 (210 mmol/L mannitol, 70 mmol/L sucrose, 5 mmol/L HEPES, 1 mmol/L EGTA and 0.5% (w/v) fatty acid-free bovine serum albumin) and homogenized (Qiagen tissueruptor, Cat. No. 9001271, Limburg, CA) for 10 sec at the lowest speed on ice. The homogenate was centrifuged at 600×*g* for 5 min at 4°C and the supernatant was transferred to new microfuges tubes centrifuged at 5000×*g* for 5 min at 4°C. After discarding the supernatant, the mitochondrial pellet was resuspended in 1 mL mitochondrial assay solution (1X-MAS, pH7.2: 220 mmol/L mannitol, 70 mmol/L sucrose, 5 mmol/L $MgCl_2$, 2 mmol/L HEPES, 10 mmol/L KH_2PO_4, 1 mmol/L EGTA, 0.2% (w/v) fatty acid-free BSA). Mitochondrial fractions were isolated and the total protein concentrations were determined as previously (26). Non-mitochondrial contaminants from lysosomes and peroxisomes (30) in the mitochondrial pellets were confirmed by immunoblotting using antibodies against lysosome-associated membrane protein 1 (LAMP-1) and catalase, respectively, while ATP synthase α subunit 1 (ATP5A1) and citrate synthase were used as mitochondrial markers.

Mitochondrial respiration assay

Freshly isolated mitochondria were then used to assess cellular respiration using a coupled assay to determine mitochondrial ETC efficiency and proton leak (30). All processing steps were conducted on ice unless otherwise indicated. Briefly, diluted isolated mitochondria (4 μg protein/90 μL 1X- MAS) were loaded into individual wells of a Seahorse *XFe* 96 cell culture microplate. The pre-warmed (37°C) coupling substrates solution composed of 1X-MAS supplemented with 10 mmol/L pyruvate, 10 mmol/L malate and 10 mmol/L succinate was added into each cell. The oxygen consumption rate (OCR) of isolated hepatic mitochondria was measured using the Extracellular Flux *XFe* 96 Analyzer according to the manufacturer's instructions (Seahorse Bioscience Inc., North Billerica, MA). Injections were as follows: Port A, 20 μL of 40 mmol/L ADP (4 mmol/L final concentration); Port B, 22 μL of 15 μmol/L oligomycin (OLIGO, 1.5 μmol/L final concentration); Port C, 24 μL of 40 μmol/L carbonilcyanide *p*-triflouromethoxyphenylhydrazone (FCCP, 4 μmol/L final concentration); Port D, 26 μL of 40 μmol/L antimycin A (AA, 4 μmol/L final concentration). The basal reading of OCR determined the basal respiration rate, while the difference between the OCR reading after OLIGO and AA injections were used to calculate the proton leak. The non-mitochondrial respiration OCR reading was eliminated from the coupling OCR readings (for additional details, see Supplemental Fig. S1A, the original Seahorse OCR graph enclosed as supplemental Fig. S1C, biomarkers for the lysosomes and peroxisomes shown in supplemental Fig. 1E). To measure electron flow through the electron transport chain, pre-warmed (37°C) electron flow substrate solution containing 1X-MAS supplemented with 10 mmol/L pyruvate, 10 mmol/L malate and 4 μmol/L FCCP. The injection protocol for electron flow was as follows: Port A, 20 μL of 20 μmol/L rotenone (2 μmol/L final concentration); Port B, 22 μL of 100 mmol/L succinate (1.5 μmol/L final concentration); Port C, 24 μL of 40 μmol/L AA (4 μmol/L final concentration); Port D, 26 μL of 100 mmol/L ascorbate/1 mmol/L 5,10,15,20-tetrakis(2,4,6-trimethylphenyl)porphyrin (TMP) (final concentrations of 10 mmol/L and 100 μmol/L, respectively). The OCR difference before and after rotenone injection was used to determine the capacity of complex

I capacity. The OCR difference before and after AA administration reflected the complex II capacity, and the capacity of complex IV was calculated by subtracting OCR post-AA injection from the OCR post-ascorbate/TMP. The non-mitochondrial respiration OCR reading was substrated from the electron flow OCR readings (for additional details, see Supplemental Fig. S1B, the original Seahorse OCR graph enclosed as supplemental Fig. S1D. The instrumental and injection protocols for both mitochondrial functional assays is described in the Supplemental Table S1.

Detection of mitochondrial protein carbonylation

Mitochondrial protein carbonylation was detected as described (31) using an OxyBlot protein oxidation detection kit (catalog # S7150, EMD Millipore, Temecula, CA, USA) according to the manufacturer's instructions. Protein samples were reacted with 2,4-dinitrophenylhydrazine (DNP-hydrazine, DNPH) to derivatize the carbonyl groups to 2,4-dinitrophenylhydrazone (DNP-hydrazone). Samples without DNPH treatment were used as a negative control (background). The DNPH-treated and non-treated samples were separated electrophoretically on SDS-PAGE followed by Western blotting using anti-DNP antibody. Total protein loading was normalized using succinate dehydrogenase subunit α (SDHA) as a loading control.

Mitochondrial proteomics and bioinformatics analysis

Hepatic mitochondria from fresh tissues were isolated by use of a Qproteome mitochondrial isolation kit (Qiagen, Limburg, CA) and used for the mitochondrial proteomics and aconitase activity assay. Equal amounts of mitochondrial samples (25.0 μg/sample) were digested with trypsin using standard methodologies, and the resulting peptides were analyzed by LC-MS/MS on an LTQ-OrbitrapXL mass spectrometer as previously described (32) using 40 cm analytical columns. Extracts from each mouse (n=3/group) were analyzed at four technical replicates. The resulting data were used for Mascot searching against mouse sequences in the Uniprot protein sequence database (> 46,000 sequences). Search results were validated using the Peptide Prophet and Protein Prophet algorithms in Scaffold (Proteome Software, Inc, Portland, OR), using a cut-off threshold of < 1% protein and peptide false discoveries. The resulting proteins were quantitated by spectrum counting. Proteins that were differentially expressed at a significant level were selected with the P value smaller than 0.05 using a two-tailed student's t-test.

The DAVID 6.7 Bioinformatics tool (http://david.abcc.ncifcrf.gov/) was used for gene functional categorization. The proteins from mitochondrial proteomic data showing significant changes in expression were loaded into DAVID and analyzed to determine protein functional annotation to identify GO (gene-gene ontology) categories of protein functions that were enriched in the set of differentially expressed proteins based on these selected proteins (33). The selected protein functional analysis was also conducted by Ingenuity Pathway Analysis (IPA) which provided canonical pathways, upstream regulator analysis, top Toxicity (Tox) analysis and downstream effects analysis based on these selected proteins (34, 35).

Mitochondrial aconitase activity assay

Hepatic mitochondrial samples from the preparation above using a Qproteome mitochondrial isolation kit (Qiagen, Limburg, CA) were also subjected to the mitochondrial aconitase activity assay according to the manufacturer's instruction (Biovision Inc., catalog # K716-100, http://www.biovision.com/aconitase-activity-colorimetric-assay-kit-2947.html, Milpitas, CA, USA). The activity was expressed as mU/mg protein.

Immunoblot Analysis

Proteins were extracted from liver tissues and/or isolated mitochondria with the lysis buffer containing 20 mmol/L Tris-HCl (pH 7.5), 0.5 mmol/L EDTA, 0.5 mmol/L EGTA, 0.5% (v/v) Triton X-100, and 0.1% (v/v) protease and phosphatase inhibitor cocktails, respectively (Sigma-Aldrich). Immunoblot analysis was conducted as previously described (24, 25). Total pixel intensity of each protein band was normalized to a loading control for graphing and statistical analysis. Antibodies against fatty acid synthase (FASN) (catalog # 10624-2-Ap), ATP synthase α subunit 1 (ATP5A1) (catalog # 14676-1-AP), citrate synthase (catalog # 16131-1-AP), hydroxyacyl-coenzyme A dehydrogenase (HADH) (catalog # 19828-1-AP), succinate dehydrogenase α (SDHA) (catalog # , 14865-1-AP), and nicotinamide nucleotide transhydrogenase (NNT) (catalog # 13442-2-AP) were purchased from ProteinTech Group (Chicago, IL, USA); Antibodies against lysosome-associated membrane protein 1 (LAMP1) (catalog # sc-20011), catalase (catalog # sc-50508), NNT (catalog # sc-163154), glutathione reductase (GSR) (catalog # sc-133245) were purchased from Santa Cruz Biotech (Dallas, TX, USA); peroxisome proliferator-activated receptor α (PPARα) antibody (catalog # 101710) was purchased from Cayman (Ann Arbor, MI, USA); Antibodies against β-actin (catalog # 4967), phosphor-Thr172-AMP-activated protein kinase α (pT172-AMPKα) (catalog # 2535), and AMPKα (catalog # 2603) were purchased from Cell Signaling Technology (Danvers, MA, USA); voltage-dependent anion-selective channel protein 1 (VDAC1) antibody (catalog # PA1780) was purchased from Boster Biosciences (Pleasanton, CA, USA).

Statistical analysis

The results from the mitochondrial respiration assay were analyzed by the *XFe* wave software (Seahorse Bioscience Inc., MA), and displayed as OCR (pmol/μg protein/min). Experimental results were analyzed by student's t-test. Data were presented as mean ± SD, n=6, unless otherwise stated in the text. Significance was set at $P < 0.05$. p values were corrected for multiple testing.

Results

Overall nutrient metabolism is changed in BCO2 KO mice

β–carotene 15, 15'-oxygenase 1 (BCO1) protein level was not altered in BCO2 KO compared to WT mice (data not shown). The daily food intake was measured from postnatal week 3 to week 6, and the result showed that BCO2 KO mice consumed more chow diet (by 15–18 %) compared to the WT, for instance, the daily food intake between 5 and 6 weeks of age was significantly higher in BCO2 KO (2.6 ± 0.1 g/mouse/day) than WT mice (2.2 ± 0.1

g/mouse/day) (n=12 mice/group, p <0.001). Interestingly, despite a significantly higher food intake, the body weight of BCO2 KO mice at 6 weeks of age (18.6 ± 1.5 g) was significantly lower (by approximately 12 %), compared to age-matched WT mice (21.2 ± 1.0 g) ($p < 0.01$, n=12 mice/group).The higher fasting blood glucose (70.2 ± 13.15 mg/dL in WT vs 111.67 ± 10.50 mg/dL in KO, $p<0.001$, n=12 mice/group) and FFA levels (0.70 ± 0.11 mEq/L in WT vs 0.95 ± 0.06 mEq/L in KO, $p<0.01$, n=6 mice/group) were observed in male BCO2 KO mice at 6 weeks of age, compared to the age and gender matched WT. Further, PPARα and AMPK, two key proteins in the energy metabolism pathway (36, 37) were analyzed by immunoblotting. The protein level of hepatic PPARα was significantly decreased in the BCO2 KO compared to the WT mice (Fig. 1 A and B). Additionally, the activation of AMPK, as indicated by phosphorylation of Thr172 in the AMPKα catalytic domain was significantly lower in the liver of BCO2 KO compared to WT mice (Fig. 1 A and C). Moreover, the elevated expression of fatty acid synthase protein (FASN, Fig. 1 A and D) was found in liver of BCO2 KO mice, compared to WT.

Mitochondrial proton leak, basal respiration rate, and capacity of complex II are altered in BCO2 KO mice

Mitochondrial function was measured via mitochondrial coupling and electron flow assays. These analyses revealed significant increases in the basal respiration rate, proton leak (Fig. 2A), and complex II capacity (Fig. 2B) in BCO2 KO compared to WT mice.

The mitochondrial proteome is changed in BCO2 KO mice

In order to determine potential mechanisms by which mitochondrial functional changes were associated with mitochondrial protein expression in BCO2 KO mice, a comparison of the WT and BCO2 KO hepatic mitochondrial proteomes was performed (n=3 mice/group with 4 technical replicates/mouse). Thirty four mitochondrial proteins were identified to have significant changes with 13 proteins being up-regulated and 21 proteins being down-regulated in the hepatic mitochondrial fractions of BCO2 KO compared to WT mice ($p < 0.05$) (Table 1). Bioinformatic analysis using DAVID functional annotation tools revealed that fatty acid oxidation, amino acid metabolism, the tricarboxylic acid (TCA) cycle, and the electron transport chain (ETC)/oxidative phosphorylation (OXPHOS) were affected most in BCO2 KO mice, which are all related to energy metabolism. The detailed results were summarized in Table 1. The raw MS/MS data were uploaded as the online supplemental materials (Supplemental Table S2). Differences revealed by proteomic analysis were confirmed by immunoblot analysis for the mitochondrial proteins, hydroxyacyl-coenzyme A dehydrogenase (HADH), voltage-dependent anion-selective channel protein 1 (VDAC1) (Supplemental Fig. S2A and B), and nicotinamide nucleotide transhydrogenase (NNT) (Fig. 3C).

The mitochondrial proteome data were also subjected to the IPA Top Tox analysis indicating that mitochondrial function and oxidative phosphorylation were mostly affected in BCO2 KO liver (Proteomic raw data enclosed as the online Supplemental Table S2, Supplemental Table S3). In ETC/OXPHOS, the expression of proteins of mitochondrial complex I, complex II, complex IV and complex V was diminished in BCO2 KO mice compared to WT

mice, whereas cytochrome *c* was increased in the BCO2 KO compared to the WT mice (Supplemental Fig. S3A).

Elevated cellular oxidative stress in the liver of BCO2 KO mice

The results in Fig. 3A showed a significant elevation of the ROS level in hepatic homogenates from the BCO2 KO (0.63 ± 0.08 OD 485/530 (relative fluorescent unit)), as compared to the WT (0.45 ± 0.03 OD 485/530 (relative fluorescent unit)) (n=6 mice/group, $p < 0.05$). In parallel, the mitochondrial proteomic data also showed elevation of oxidative stress in the liver of KO mice. For instance, the antioxidant enzymes, manganese superoxide dismutase (SOD2) (Table 1) and glutathione-disulfide reductase (glutathione reductase, GSR) (Fig. 3B) were both repressed. In contrast, the levels of peroxiredoxin 3 (PRX3) and PRX5 (38, 39) (Supplemental Fig. S3B), and nicotinamide nucleotide transhydrogenase (NNT) (Table 1, and Fig. 3C), were increased significantly in BCO2 KO compared to WT mice. Furthermore, the mitochondrial protein carbonylation levels were much higher in BCO2 KO than those in WT mice (Fig. 3D). Mitochondrial aconitase is an iron-sulfur protein containing a $[4Fe\text{-}4S]^{2+}$ cluster in its active site that catalyzes the stereospecific dehydration–rehydration in the TCA cycle. It has been considered as a measure of oxidative damage (40). The result revealed that the mitochondrial aconitase activity was also declined in BCO2 KO mice (Fig. 3E). Collectively, the results indicated hepatic mitochondrial dysfunction and cellular oxidative stress in BCO2 KO mice.

4. Discussion

Mitochondrial dysfunction has been considered one of the major causal factors in the development of chronic diseases such as obesity, type 2 diabetes, and other metabolic disorders (40, 41). BCO2 resides in the inner mitochondrial membrane. In this study, the impact of BCO2 on mitochondrial function was investigated using WT and BCO2 KO mice. Importantly, there was no changes in either BCO1 protein level, hepatic retinol and retinal contents (data not shown), or accumulation of carotenoids (including β–carotene, α-carotene, β-cryptoxanthin, lutein, zeaxanthin, and lycopene) observed in the liver of BCO2 KO mice fed a standard chow diet (data not shown), suggesting that the loss of BCO2 did not affect hepatic vitamin A and carotenoid metabolism at 6 weeks of age, if there was any trace carotenoids in the diet. Whether this observation indicates the presence of a compensatory pathway or that it takes longer than 6 weeks to accumulate carotenoids remains unclear. Despite no apparent changes in carotenoid metabolism, the loss of BCO2 triggered alterations in various metabolic pathways including, but not limited to fatty acid oxidation, TCA cycle, and ETC/OXPHOS. Alterations in these pathways likely contributed to increased oxidative stress and elevation of fasting blood glucose and FFA levels that were observed in BCO2 KO mice and indicated an unknown role of BCO2 that was independent of its enzymatic carotenoid cleavage function.

Food intake is dynamic and regulated largely by whole-body energy metabolism and circadian rhyme. In this present study, the loss of BCO2 was hypothesized to result in mitochondrial dysfunction and contribute to the disturbance of energy metabolism in mice. Based on the proteomics analysis, the expression of ETC/OXPHOS complex I, II, and IV

proteins was reduced in the livers of BCO2 KO mice, though the expression of cytochrome *c* was increased in the BCO2 KO, compared to WT mice. These observations may suggest that a change of mitochondrial proteome occurred in BCO2 KO mice (42–49). Decreased protein expression of the mitochondrial proteome has been linked to hyperactivation of hepatic mitochondria in diabetes and obesity (13, 46). The low aconitase activity occurs in obese mice with higher mitochondrial respiration activities (44). Ischemic hearts have a lower mitochondrial complex OCR activity though the mitochondrial complex I protein contents are higher (42). Mitochondria are far more complex in form and function than anticipated and are controlled by multiple factors such as circadian, nutrient availability (e.g., fasting and fed), and protein expressions (47, 49). Despite this potential compensatory mechanism of mitochondrial changes in BCO2 KO animals, the increased proton leak from the mitochondrial inner membrane space into the matrix observed in this study indicated the possibility that energy efficiency was impaired in BCO2 KO mice (50, 51).

Hyperactivation of mitochondrial respiration links to oxidative stress and metabolic disorders. Deficiency of BCO2 caused changes of the mitochondrial proteome and hyperactivation of the mitochondrial function in BCO2 KO mice. The results further demonstrated that hepatic cells experienced mitochondrial and cellular oxidative stress as shown in Fig. 3. Increased respiratory capacity of complex II leads to overproduction of ROS (52), which could also be supported by the result on the mitochondrial protein carbonylation (Fig. 3D). Oxidative stress leads to modification of native amino acid residues in proteins to carbonyl derivatives known as protein carbonylation (31). Indeed, the elevation of ROS production could further impair mitochondrial function (53).

Elevated ROS can be eliminated by a variety of enzymes and/or antioxidants, such as SOD, catalase, glutathione peroxidase (GPx) and glutathione (GSH). GSR catalyzes the reduction of glutathione disulfide (GSSG) to regenerate the sulfhydryl for GSH. NNT is a key mitochondrial antioxidant enzyme, utilizing the mitochondrial proton gradient to generate NADPH from NADH and $NADP^+$ (54, 55). In this study, enhanced expression of NNT protein (two bands in BCO2 KO mice shown by immunoblotting) might suggest that BCO2 depletion might cause the altered expression of NNT variants under oxidative stress (56). It is clear that a mild increase in mitochondrial ROS production induces activation of long-lasting cytoprotective pathways, for instance activation of antioxidant enzymes (57), while pro-longed and/or severe oxidative stress results in suppression of a large variety of gene expression, including antioxidant enzymes, such as mitochondrial SOD2 (57, 58). Genetic depletion of BCO2 triggered mitochondrial and subsequent cellular oxidative stress which might account for decreased expression of SOD2, GSR, and other antioxidants. The reduction of GPx level would in turn conserve GSH in favor of forming GSSG. The further study is warranted to confirm the hypothesis above. Elevation of blood glucose and free fatty acids could also be considered as additional markers of disruption of nutrient metabolism and oxidative stress in BCO2 KO mice.

In conclusion, the results presented herein indicated that the loss of BCO2 was associated with changes of the hepatic mitochondrial proteome and function shown a decrease in the ETC efficiency and increases in proton leak, basal respiration activity, and complex II capacity– all of which could contribute to mitochondrial hyperactivation and subsequently

mitochondrial and cellular oxidative stress. That in turn led to mitochondrial energy insufficiency and disruption of nutrient metabolism in BCO2 KO, compared to WT mice (Fig. 4). The findings suggested that BCO2 may play a structural role in the inner membrane of mitochondria through regulation of the ETC complexes activity, and/or metabolize unknown substrates that subsequently altered mitochondrial function. Further studies are warranted to determine if BCO2 represents a potential therapeutic target to reduce the risk of or impact chronic oxidative stress associated with diseases such as diabetes, obesity, and cardiovascular disease.

Supplementary Material

Refer to Web version on PubMed Central for supplementary material.

Acknowledgments

Acknowledgment/funding

Mass spectrometry analyses were performed in the DNA/Protein Resource Facility at Oklahoma State University, using resources supported by the NSF MRI and EPSCoR programs (award DBI/0722494). This project was made possible in part by support from the USDA National Institute of Food and Agriculture 2015-67018-23176, USDA NIFA Hatch Project OKL02992, National Institute of General Medical Sciences of the National Institutes of Health under Award Number P20GM103648, and Oklahoma State University faculty start-up project (to DL)

Abbreviations

AMPK	AMP-activated protein kinase
ATP5A1	ATP synthase α subunit 1
BCO1	β–carotene-15, 15’-oxygenase 1
BCO2	β, β-carotene-9’, 10’-dioxygenase 2
BHMT	betaine homocysteine methyltransferase
DMG	dimethylglycine
ETC	electron transport chain
FASN	fatty acid synthase
GS	glutathione synthetase
GSH	glutathione
GSR	glutathione disulfide reductase
GSSG	glutathione disulfide
HADH	hydroxyacyl-coenzyme A dehydrogenase
HSP60	heat shock protein 60
IL-18	interleukin 18

IPA	ingenuity pathway analysis
KO	knockout
LAMP1	lysosome-associated membrane protein 1
MAS	mitochondrial assay solution
NNT	nicotinamide nucleotide transhydrogenase
OCR	oxygen consumption rate
OXPHOS	oxidative phosphorylation
PPAR	peroxisome proliferator-activated receptor
PRX	peroxiredoxin
ROS	reactive oxygen species
SDHA	succinate dehydrogenase α
SOD	superoxide dismutase
SOD2	manganese superoxide dismutase, mitochondria
TCA	tricarboxylic acid cycle
VDAC1	voltage-dependent anion-selective channel protein 1
WT	wild type

References

1. Hybertson BM, Gao B, Bose SK, McCord JM. Oxidative stress in health and disease: the therapeutic potential of Nrf2 activation. Mol. Aspects Med. 2011; 32:234–246. [PubMed: 22020111]
2. Borges CG, Canani CR, Fernandes CG, Zanatta A, Seminotti B, Ribeiro CA, Leipnitz G, Vargas CR, Wajner M. Reactive nitrogen species mediate oxidative stress and astrogliosis provoked by in vivo administration of phytanic acid in cerebellum of adolescent rats: A potential contributing pathomechanism of cerebellar injury in peroxisomal disorders. Neurosci. 2015; 304:122–132.
3. Negi R, Pande D, Karki K, Kumar A, Khanna RS, Khanna HD. Association of oxidative DNA damage, protein oxidation and antioxidant function with oxidative stress induced cellular injury in pre-eclamptic/eclamptic mothers during fetal circulation. Chem-biol. Interactions. 2014; 208:77–83.
4. Czabotar PE, Lessene G, Strasser A, Adams JM. Control of apoptosis by the BCL-2 protein family: implications for physiology and therapy. Nat. Rev. Mol. Cell. Biol. 2014; 15:49–63. [PubMed: 24355989]
5. Starkov AA. The role of mitochondria in reactive oxygen species metabolism and signaling. Ann. New York Acad. Sci. 2008; 1147:37–52. [PubMed: 19076429]
6. Williams GS, Boyman L, Chikando AC, Khairallah RJ, Lederer WJ. Mitochondrial calcium uptake. Proc. Natl. Acad. Sci. U. S. A. 2013; 110:10479–10486. [PubMed: 23759742]
7. Hoss SE, Bahr GM, Echtay KS. Lopimune-induced mitochondrial toxicity is attenuated by increased uncoupling protein-2 level in treated mouse hepatocytes. Biochem. J. 2015; 468:401–407. [PubMed: 26173235]
8. Bae J, Ricciardi CJ, Esposito D, Komarnytsky S, Hu P, Curry BJ, Brown PL, Gao Z, Biggerstaff JP, Chen J, et al. Activation of pattern recognition receptors in brown adipocytes induces inflammation

and suppresses uncoupling protein 1 expression and mitochondrial respiration. Am. J. Physiol. Cell Physiol. 2014; 306:C918–30. [PubMed: 24627558]

9. Thrush AB, Zhang R, Chen W, Seifert EL, Quizi JK, McPherson R, Dent R, Harper ME. Lower mitochondrial proton leak and decreased glutathione redox in primary muscle cells of obese diet-resistant versus diet-sensitive humans. J. Clin. Endocrinol. Metab. 2014; 99:4223–4230. [PubMed: 25148230]
10. Crescenzo R, Bianco F, Mazzoli A, Giacco A, Liverini G, Iossa S. Alterations in proton leak, oxidative status and uncoupling protein 3 content in skeletal muscle subsarcolemmal and intermyofibrillar mitochondria in old rats. BMC Geriatrics. 2014; 14:79. [PubMed: 24950599]
11. Brownlee M. Biochemistry and molecular cell biology of diabetic complications. Nature. 2001; 414:813–820. [PubMed: 11742414]
12. Furukawa S, Fujita T, Shimabukuro M, Iwaki M, Yamada Y, Nakajima Y, Nakayama O, Makishima M, Matsuda M, Shimomura I. Increased oxidative stress in obesity and its impact on metabolic syndrome. J. Clin. Invest. 2004; 114:1752–1761. [PubMed: 15599400]
13. Bugger H, Chen D, Riehie C, Soto J, Theobald H, H X, et al. Tissue-specific remodeling of the mitochondrial proteome in type 1 diabetic Akita mice. Diebetes. 2009; 58:1986–1997.
14. Rudich A, Tirosh A, Potashnik R, Hemi R, Kanety H, Bashan N. Prolonged oxidative stress impairs insulin-induced GLUT4 translocation in 3T3-L1 adipocytes. Diabetes. 1998; 47:1562–1569. [PubMed: 9753293]
15. Maddux BA, See W, Lawrence JC Jr, Goldfine AL, Goldfine ID, Evans JL. Protection against oxidative stress-induced insulin resistance in rat L6 muscle cells by mircomolar concentrations of alpha-lipoic acid. Diabetes. 2001; 50:404–410. [PubMed: 11272154]
16. Keaney JF Jr, Larson MG, Vasan RS, Wilson PW, Lipinska I, Corey D, Massaro JM, Sutherland P, Vita JA, Benjamin EJ, et al. Obesity and systemic oxidative stress: clinical correlates of oxidative stress in the Framingham Study. Arterioscler. Thromb. Vasc. Biol. 2003; 23:434–439. [PubMed: 12615693]
17. Babino D, Palczewski G, Widjaja-Adhi MA, Kiser PD, Golczak M, von Lintig J. Characterization of the role of β-carotene 9,10-dioxygenase in macular pigment metabolism. J. Biol. Chem. 2015; 290:24844–24857. [PubMed: 26307071]
18. Palczewski G, Amengual J, Hoppel CL, von Lintig J. Evidence for compartmentalization of mammalian carotenoid metabolism. FASEB J. 2014; 28:4457–4469. [PubMed: 25002123]
19. Li B, Vachali PP, Gorusupudi A, Shen Z, Sharifzadeh H, Besch BM, Nelson K, Horvath MM, Frederick JM, Baehr W, et al. Inactivity of human beta, beta-carotene-9',10'-dioxygenase (BCO2) underlies retinal accumulation of the human macular carotenoid pigment. Proc. Natl. Acad. U. S. A. 2014; 111:10173–10178.
20. He M, Cornelis MC, Kraft P, van Dam RM, Sun Q, Laurie CC, Mirel DB, Chasman DI, Ridker PM, Hunter DJ, et al. Genome-wide association study identifies variants at the IL18-BCO2 locus associated with interleukin-18 levels. Arterioscler. Thromb. Vasc. Biol. 2010; 30:885–890. [PubMed: 20150558]
21. Meyers KJ, Mares JA, Igo RP Jr, Truitt B, Liu Z, Millen AE, Klein M, Johnson EJ, Engelman CD, Karki CK, et al. Genetic evidence for role of carotenoids in age-related macular degeneration in the Carotenoids in Age-Related Eye Disease Study (CAREDS). Invest. Ophthalmol. Vis. Sci. 2014; 55:587–599. [PubMed: 24346170]
22. Brocato J, Hernandez M, Laulicht F, Sun H, Shamy M, Alghamdi MA, et al. In vivo exposures to particulate matter collected from Saudi Arabia or nickel chloride display similar dysregulation of metabolic syndrome genes. J. Toxicol. Environ Health A. 2015; 78:1421–1436. [PubMed: 26692068]
23. Gong X, Marisiddaiah R, Zaripheh S, Wiener D, Rubin LP. Mitochondrial beta-carotene 9, 10 oxygenase modulates prostate cancer growth via NF-kappa B inhibition: a lycopene-independent function. Mol. Cancer Res. 2016 Jul 12. pii: molcanres.0075.2016.
24. Lobo GP, Isken A, Hoff S, Babino D, von Lintig J. BCDO2 acts as a carotenoid scavenger and gatekeeper for the mitochondrial apoptotic pathway. Develop. 2012; 139:2966–2977.
25. Yu H, Wark L, Ji H, Willard L, Jaing Y, Han J, He H, Ortiz E, Zhang Y, Medeiros DM, et al. Dietary wolfberry upregulates carotenoid metabolic genes and enhances mitochondrial biogenesis

in the retina of db/db diabetic mice. Mol. Nutr. Food Res. 2013; 57:1158–1169. [PubMed: 23505020]

26. Lin D, He H, Ji H, Willis J, Willard L, Jiang Y, Medeiros DM, Wark L, Han J, Liu Y, et al. Wolfberries potentiate mitophagy and enhance mitochondrial biogenesis leading to prevention of hepatic steatosis in obese mice: the role of AMP-activated protein kinase alpha2 subunit. Mol. Nutr. Food Res. 2014; 58:1005–1015. [PubMed: 24449471]
27. Kiefer C, Hessel S, Lampert JM, Vogt K, Lederer MO, Breithaupt DE, von Lintig J. Identification and characterization of a mammalian enzyme catalyzing the asymmetric oxidative cleavage of provitamin A. J. Biol. Chem. 2001; 276:14110–14116. [PubMed: 11278918]
28. Lindqvist A, He YG, Andersson S. Cell type-specific expression of beta-carotene 9',10'-monooxygenase in human tissues. J. Histochem. Cytochem. 2005; 53:1403–1412. [PubMed: 15983114]
29. Amengual J, Lobo GP, Golczak M, Li HN, Klimova T, Hoppel CL, Wyss A, Palczewski K, von Lintig J. A mitochondrial enzyme degrades carotenoids and protects against oxidative stress. FASEB J. 2011; 25:948–959. [PubMed: 21106934]
30. Guo Y, Darshi M, Ma Y, Perkins GA, Shen Z, Haushalter KJ, et al. Quantitative proteomic and functional analysis of liver mitochondria from high fat diet (HFD) diabetes mice. Mol. Cell. Proteomics. 2013; 12:3744–3758. [PubMed: 24030101]
31. Dalle-Donne I, Rossi R, Giustarini D, Milzani A, Colombo R. Protein carbonyl groups as biomarkers of oxidative stress. Clin. Chim. Acta. 2003; 329:23–38. [PubMed: 12589963]
32. Voruganti S, Lacroix JC, Rogers CN, Rogers J, Matts RL, Hartson SD. The anticancer drug AUY922 generates a proteomics fingerprint that is highly conserved among structurally diverse Hsp90 inhibitors. J. Proteome Res. 2013; 12:3697–3706. [PubMed: 23763277]
33. Huang da W, Sherman BT, Lempicki RA. Systematic and integrative analysis of large gene lists using DAVID bioinformatics resources. Nat. Protoc. 2009; 4:44–57. [PubMed: 19131956]
34. Yu F, Shen XY, Fan L, Yu ZC. Genome-wide analysis of genetic variations assisted by Ingenuity Pathway Analysis to comprehensively investigate potential genetic targets associated with the progression of hepatocellular carcinoma. Eur. Rev. Med. Pharmacol. Sci. 2014; 18:2102–2108. [PubMed: 25070813]
35. Kramer A, Green J, Pollard J Jr, Tugendreich S. Causal analysis approaches in Ingenuity Pathway Analysis. Bioinformatics. 2014; 30:523–530. [PubMed: 24336805]
36. Prosdocimo DA, John JE, Zhang L, Efraim ES, Zhang R, Liao X, Jain MK. KLF15 and PPARalpha cooperate to regulate cardiomyocyte lipid gene expression and oxidation. PPAR. Res. 2015; 2015:201625. [PubMed: 25815008]
37. Fentz J, Kjobsted R, Birk JB, Jordy AB, Jeppesen J, Thorsen K, Schjerling P, Kiens B, Jessen N, Viollet B, et al. AMPKalpha is critical for enhancing skeletal muscle fatty acid utilization during in vivo exercise in mice. FASEB J. 2015; 29:1725–1738. [PubMed: 25609422]
38. Oka S, Hirai J, Yasukawa T, Nakahara Y, Inoue YH. A correlation of reactive oxygen species accumulation by depletion of superoxide dismutases with age-dependent impairment in the nervous system and muscles of Drosophila adults. Biogerontol. 2015; 16:485–501.
39. Freeman H, Shimomura K, Cox RD, Ashcroft FM. Nicotinamide nucleotide transhydrogenase: a link between insulin secretion, glucose metabolism and oxidative stress. Biochem. Soc. Trans. 2006; 34:806–810. [PubMed: 17052203]
40. Yan L-J, Levine RL, Sohai RS. Oxidative damage during aging targets mitochondrial aconitase. Proc. Natl. Acad. U.S.A. 1997; 94:11168–11172.
41. Hojlund K, Mogensen M, Sahlin K, Beck-Nielsen H. Mitochondrial dysfunction in type 2 diabetes and obesity. Endocrinol. Metab. Clin. North Am. 2008; 37:713–731. [PubMed: 18775360]
42. Liu T, Chen L, Kim E, Tran D, Phinney BS, Knowlton AA. Mitochondrial proteome remodeling in ischemic heart failure. Life Sci. 2014; 101:27–36. [PubMed: 24548633]
43. Valdecantos MP, Perez-Matute P, Gonzalez-Muniesea P, Prieto-Hontoria PL, Moreno-Aliaga MJ, Martinez JA. Lipoic acid administration prevents nonalcoholic steatosis linked to long-term high-fat feeding by modulating mitochondrial function. J. Nutr. Biochem. 2012; 23:1676–1684. [PubMed: 22464149]

44. Crescenzo R, Bianco F, Coppola P, Mazzoli A, Cigliano L, Liverini G, Iossa S. Increased skeletal muscle mitochondrial efficiency in rats with fructose-induced alteration in glucose tolerance. Br. J. Nutr. 2013; 110:1996–2003. [PubMed: 23693085]
45. Segref A, Kevei É, Pokrzywa W, Schmeisser K, Mansfeld J, Livnat-Levanon N, et al. Pathogenesis of human mitochondrial diseases is modulated by reduced activity of the ubiquitin/proteasome system. Cell Metab. 2014; 19:642–652. [PubMed: 24703696]
46. Koliaki C, Szendroedi J, Kaul K, Jelenik T, Nowotny P, Jankowiak F, et al. Adaptation of hepatic mitochondrial function in humans with non-alcoholic fatty liver is lost in steatohepatitis. Cell Metab. 2015; 21:739–746. [PubMed: 25955209]
47. Neufeld-Cohen A, Robles MS, Aviram R, Manella G, Adamovich Y, Ladeuix B, et al. Circadian control of oscillations in mitochondrial rate-limiting enzymes and nutrient utilization by PERIOD proteins. Proc. Natl. Acad. Sci. U. S. A. 2016; 113:E1673–1682. [PubMed: 26862173]
48. Akude E, Zherebitskaya E, Chowdhury SK, Smith DR, Dobrowsky RT, Fernyhough P. Diminished superoxide generation is associated with respiratory chain dysfunction and changes in the mitochondrial proteome of sensory neurons from diabetic rats. Diabetes. 2011; 60:288–297. [PubMed: 20876714]
49. Pagliarini DJ1, Rutter J. Hallmarks of a new era in mitochondrial biochemistry. Genes Dev. 2013; 27:2615–2627. [PubMed: 24352419]
50. Busiello RA, Savarese S, Lombardi A. Mitochondrial uncoupling proteins and energy metabolism. Front. Physiol. 2015; 6:36. [PubMed: 25713540]
51. Porter RK. Mitochondrial proton leak: a role for uncoupling proteins 2 and 3? Biochim. Biophys. Acta. 2001; 1504:120–127. [PubMed: 11239489]
52. Quinlan CL, Orr AL, Perevoshchikova IV, Treberg JR, Ackrell BA, Brand MD. Mitochondrial complex II can generate reactive oxygen species at high rates in both the forward and reverse reactions. J. Biol. Chem. 2012; 287:27255–27264. [PubMed: 22689576]
53. Cui H, Kong Y, Zhang H. Oxidative stress, mitochondrial dysfunction, and aging. J. Signal Transduction. 2012
54. Lopert P, Patel M. Nicotinamide nucleotide transhydrogenase (Nnt) links the substrate requirement in brain mitochondria for hydrogen peroxide removal to the thioredoxin/peroxiredoxin (Trx/Prx) system. J. Biol. Chem. 2014; 289:15611–15620. [PubMed: 24722990]
55. Nickel AG, von Hardenberg A, Hohl M, Loffler JR, Kohlhaas M, Becker J, Reil JC, Kazakov A, Bonnekoh J, Stadelmaier M, et al. Reversal of mitochondrial transhydrogenase causes oxidative stress in heart failure. Cell Metab. 2015; 22:472–484. [PubMed: 26256392]
56. Wong N, Blair AR, Morahan G. Andrikopoulos, The deletion variant of nicotinamide nucleotide transhydrogenease (NNT) does not affect insulin secretion or glucose tolerance. Endocrinol. 2010; 151:96–102.
57. Willems PHGM, Rossignol R, Dieteren CEJ, Purphy MP, Kopman WJH. Redox homeostasis and mitochondrial dynamics. Cell Metab. 2015; 22:207–217. [PubMed: 26166745]
58. Giu X, Brown K, Hirschey MD, Verdin E, Chen D. Calorie restriction reduces oxidative stress by SIRT3-mediated SOD2 activation. Cell Metab. 2010; 12:662–667. [PubMed: 21109198]

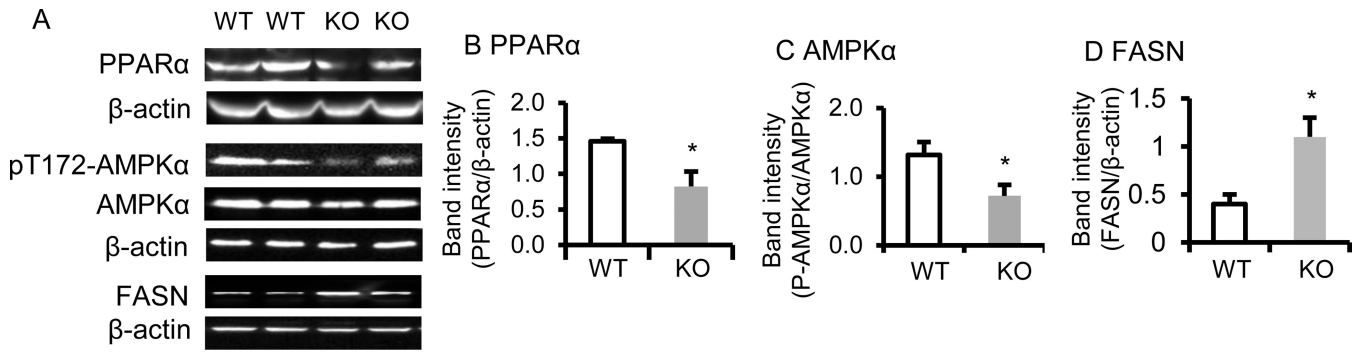

Figure 1. Expression of energy metabolism-related proteins is altered in BCO2 KO mice

The expression of hepatic PPARα protein (A and B), AMPKα and pT172-AMPKα (A and C), and FASN (A and D) were determined by immunoblotting on the left and band quantification was shown on the right. The activation of AMPKα (pT172-AMPKα / AMPKα) was reduced in the BCO2 KO mice compared to WT mice. Values are means ± SD, n=6 mice/group. * Different from WT, $p < 0.05$. KO, knockout; WT wild type. PPARα, PPAR, peroxisome proliferator-activated receptor α; AMPKα, AMP-activated protein kinase α; FASN, fatty acid synthase

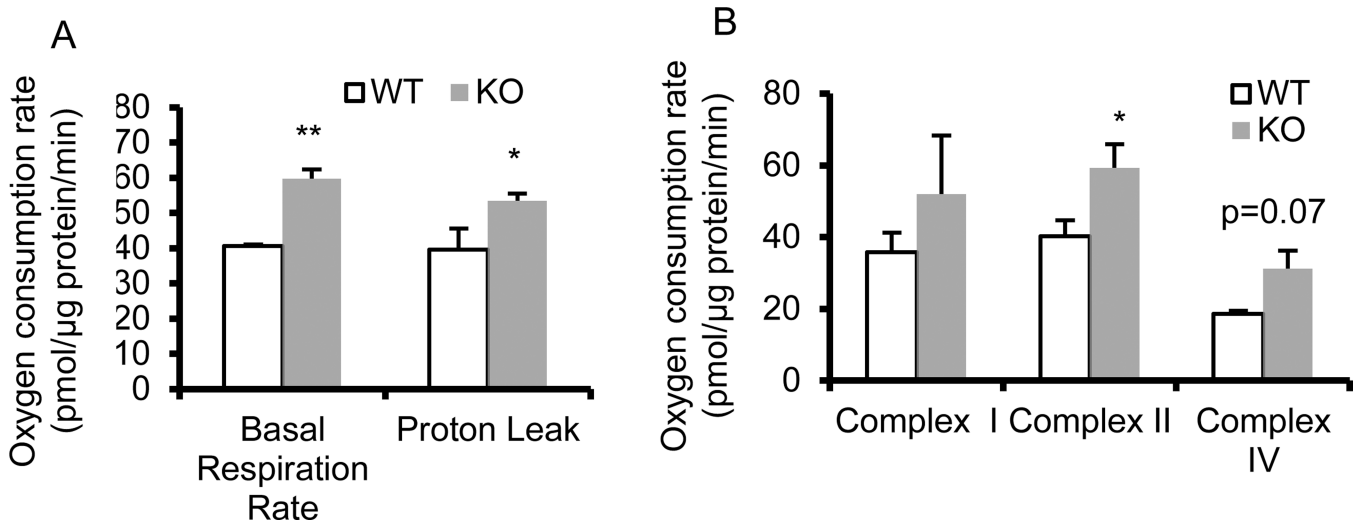

Figure 2. Functional analysis of isolated hepatic mitochondria from 6-week-old male BCO2 KO and WT mice

(A) The basal respiration rate and proton leak were increased significantly in BCO2 KO mice. (B) No change was observed in the capacities of complex I and complex IV while complex II capacity was significantly increased in BCO2 KO, compared to WT mice. Values are means ± SD, n=6 mice/group, with 6 technical replicates/mouse. * Different from WT, $p < 0.05$. ** Different from WT, $p < 0.01$. KO, knockout; WT wild type.

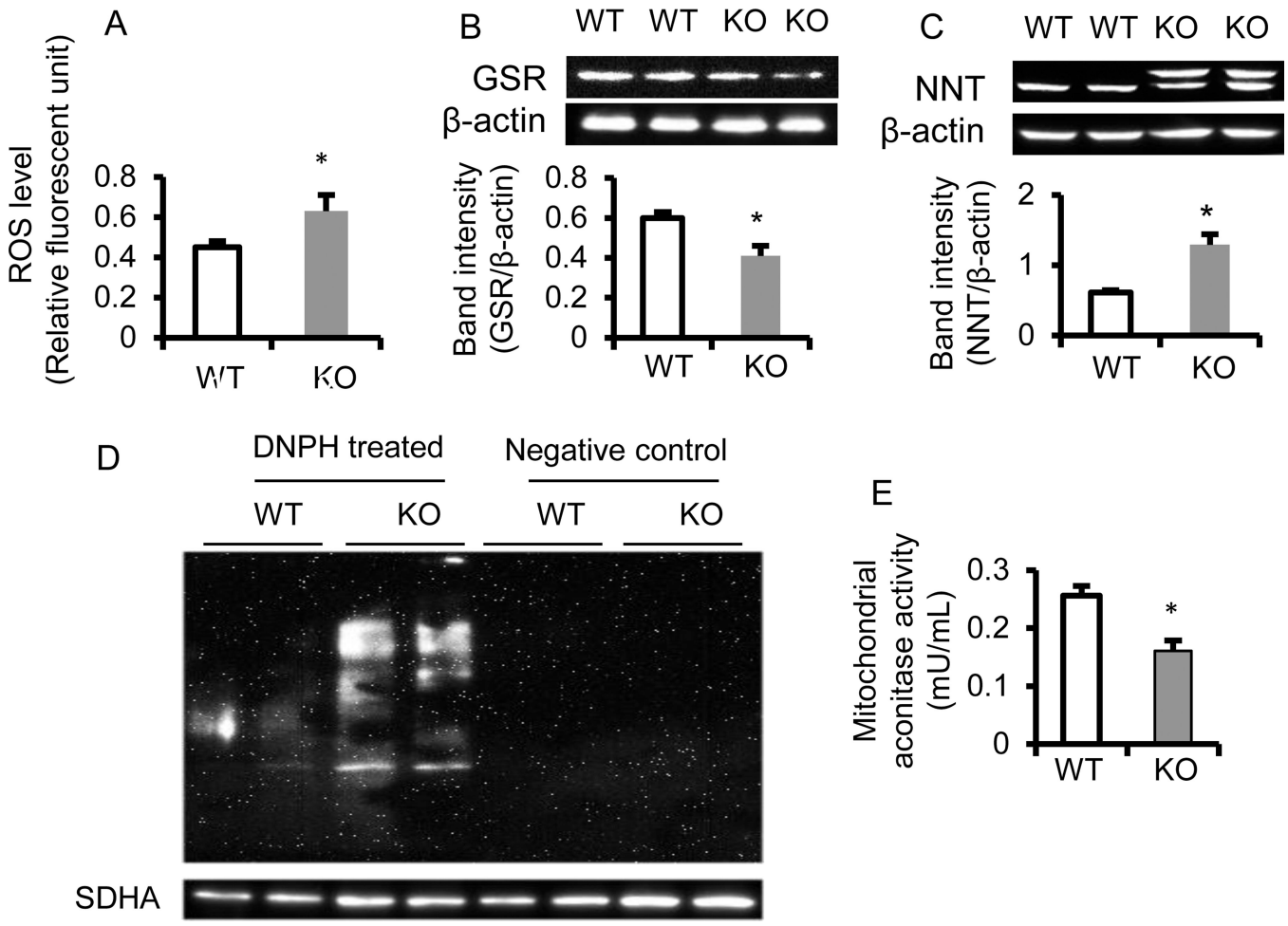

Figure 3. Cellular and mitochondrial oxidative stress are elevated in the liver of BCO2 KO compared to WT mice

The level of hepatic cellular reactive oxygen species (ROS) (A), hepatic protein expression of glutathione reductase (GSR) (B), nicotinamide nucleotide transhydrogenase (NNT) (C) by immunoblotting. Mitochondrial protein carbonylation was assessed by the OxyBlot protein oxidation detection kit (catalog # S7150, EMD Millipore, Temecula, CA, USA) according to the manufacturer's protocol (D). Succinate dehydrogenase α (SDHA) as a loading control. Hepatic mitochondrial aconitase activity was measured using an aconitase activity colormetric assay kit (Biovision Inc) (E). The results are presented as mean ±SD (n=6 mice/group, * Different from WT, $p<0.05$). KO, knockout; WT, wild type. DNPH, 2,4-dinitrophenylhydrazine

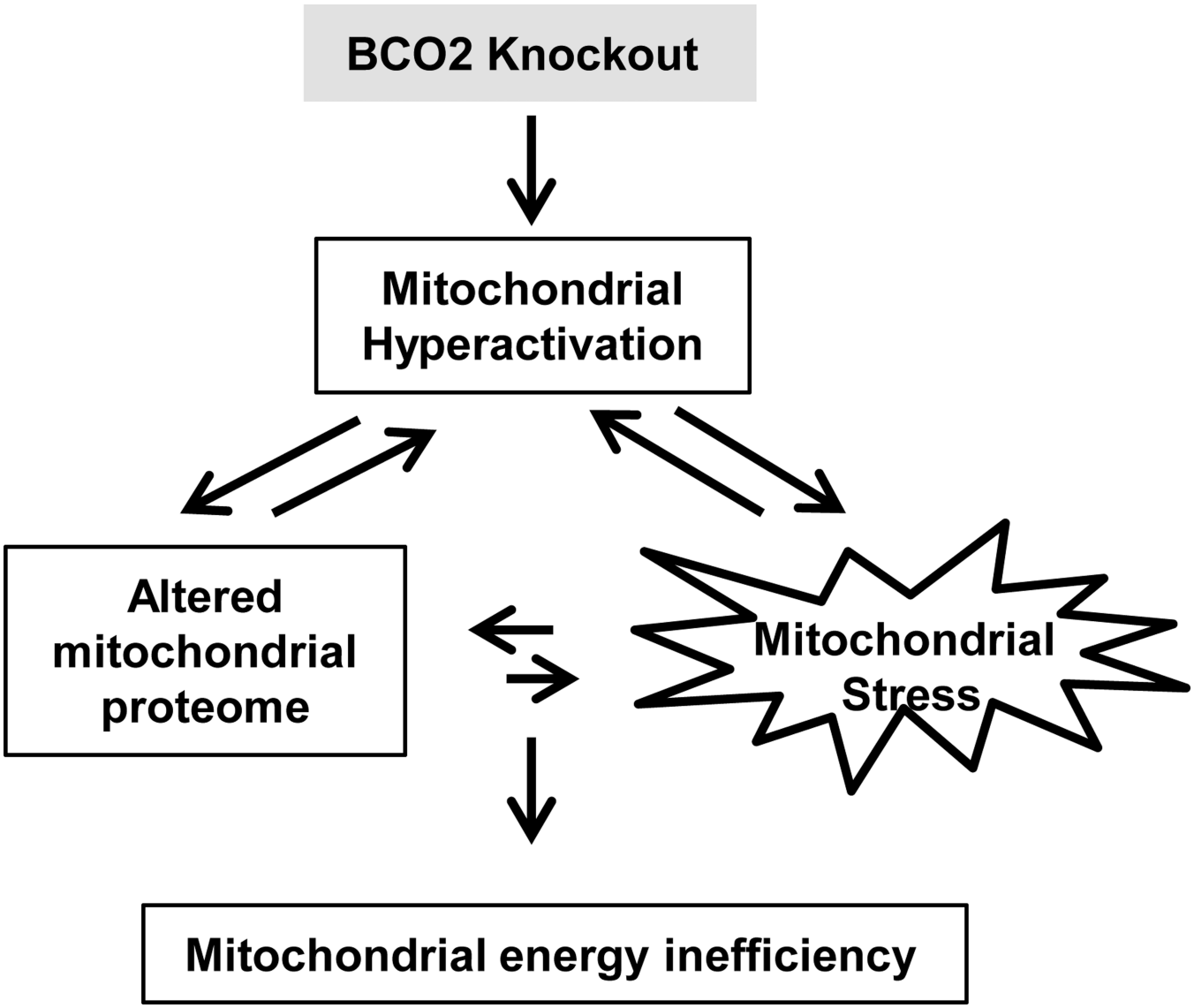

Figure 4. Schematic diagram showing the potential mechanism of BCO2 in mitochondrial function and oxidative stress

The loss of BCO2 was associated with changes of the hepatic mitochondrial proteome and function shown as a decrease in the ETC efficiency and increases in proton leak, basal respiration activity, and complex II capacity– all of which could contribute to mitochondrial hyperactivation and subsequent mitochondrial and cellular oxidative stress, which in turn led to mitochondrial energy insufficiency and disruption of nutrient metabolism in BCO2 KO, compared to WT mice

Table 1

Functional categorization of proteins differentially expressed in hepatic mitochondria of BCO2 knockout (KO) vs. 129S6 wild type (WT) mice identified by spectrum counting. Values are means, n=3 mice/group with 4 technical replicates/mouse.

Gene symbol	Protein name	Ratio(KO/WT)	p-values
Fatty Acid Metabolism			
ATP11C	Probable phospholipid-transporting ATPase 11C	0.73	0.04
HADH	Hydroxyacyl-coenzyme A dehydrogenase, mitochondrial	0.87	0.02
ECI1	Enoyl-CoA delta isomerase 1, mitochondrial	1.59	0.01
Amino Acid Metabolism			
GLDC	Glycine dehydrogenase (decarboxylating), mitochondrial	0.45	0.03
MSRA	Isoform 2 of Mitochondrial peptide methionine sulfoxide reductase	0.51	0.02
GLS2	Glutaminase liver isoform, mitochondrial	0.72	0.03
SARDH	sarcosine dehydrogenase, mitochondrial	0.83	0.02
GLYATL	Glycine N-acyltransferase-like protein	0.85	0.02
AMT	Aminomethyltransferase, mitochondrial	1.43	0.04
OAT	Ornithine aminotransferase, mitochondrial	1.69	0.03
TCA Cycle			
SUCLG2	Succinyl-CoA ligase [GDP-forming] subunit beta, mitochondrial	0.81	0.04
CS	Citrate synthase	1.24	0.01
DHTKD1	Probable 2-oxoglutarate dehydrogenase E1 component DHKTD1, mitochondrial	2.87	0.002
ETC			
NDUFA10	NADH dehydrogenase [ubiquinone] 1 alpha subcomplex subunit 10, mitochondrial	0.84	0.05
SDHA	Succinate dehydrogenase [ubiquinone] flavoprotein subunit, mitochondrial	0.87	0.03
SUOX	Sulfite oxidase, mitochondrial	1.30	0.003
NNT	NAD(P) transhydrogenase, mitochondrial	87.67/0	0.001
Mitochondria Protein Translation			
AK4	Adenylate kinase 4, mitochondrial	0.50	0.03
RPL7	ribosomal protein L7	0.72	0.004
Vitamin A and Drug Metabolism			
UGT1A5	MCG14318, isoform CRAh	0.71	0.02
CYP1A2	CYP1A2 cytochrome P450, family 1, subfamily A, polypeptide 2	1.15	0.03
CYP2D9	cytochrome P450, family 2, subfamily d, polypeptide 9	1.18	0.01
CYP2C40	Cytochrome P450 2C40	3.03	0.04
CYP7B1	25-hydroxycholesterol 7-alpha-hydroxylase	12.63	0.04
Protease			
CLPX	ATP-dependent Clp protease ATP-binding subunit clpX-like, mitochondrial	0.74	0.02
Transport Protein			

Gene symbol	Protein name	Ratio(KO/WT)	p-values
TIMM50	Mitochondrial import inner membrane translocase subunit TIM50	0.60	0.03
VDAC3	Voltage-dependent anion-selective channel protein 3	0.79	0.002
VDAC1	Isoform Mt-VDAC1 of Voltage-dependent anion-selective channel protein 1	0.91	0.01
Misc			
SOD2	Superoxide dismutase [Mn], mitochondrial	0.83	0.04
HYOU1	Hypoxia up-regulated protein 1 protein folding HSP70 family	0.84	0.05
CES2A	Pyrethroid hydrolase Ces2a	0.92	0.04
CPS1	Carbamoyl Phosphate Synthetase I	0.94	0.003
ALDH1B1	Aldehyde dehydrogenase X, mitochondrial	1.11	0.02
EPHX1	Epoxide hydrolase 1	1.13	0.05
ETHE1	Persulfide dioxygenase ETHE1, mitochondrial	1.28	0.002